# A High-Power DC-DC Converter based Dual Active Bridge for MVDC Grids on Offshore Wind Farms

Youngsil Lee, Gaurang Vakil, Ralph Feldman, Alan. J. Watson, Patrick W. Wheeler
The University Of Nottingham
University Park
Nottingham, UK
Tel.: +44 / (0) – 115.951.5151
E-Mail: eexyl30@nottingham.ac.uk
URL: http://www.nottingham.ac.uk

## Keywords

«Dual Active Bridge», «high-power dc-dc converter», «offshore wind farms », «MVDC Grids», «power loss».

## Abstract

This paper presents the steady-state analysis of a high power step-up DC-DC converter based three-phase dual active bridge (3DAB) for use as a medium voltage (MV) DC-DC collector of offshore wind farms. An optimization procedure for a high-power medium frequency transformer is explained and moreover, a design of an optimal control phase shift angle is explained and verified through simulation. The comparisons with two scenarios are presented: 4MW converters for power conversion from low dc voltage (LVDC) of the wind turbine output terminal to 40kV MVDC grid of offshore wind farms. The proposed 3DAB DC-DC converter is investigated for the given scenarios in terms of losses of the semi-conductors and the magnetic part as well as the quantity of semi-conductors.

## Introduction

Recently, DC grids have been considered as a special research topic of the power system due to the fastest growing renewable energy industries such as wind energy or solar energy. References [1-3] present many advantages of DC grids such as low power losses and small size cable for carrying large amounts of power over long distances. Furthermore, a bulky conversional 50/60Hz transformer can be replaced by medium- frequency transformers operating at the kilo-hertz range so that a considerable reduction in transformer weight/size could be achieved.

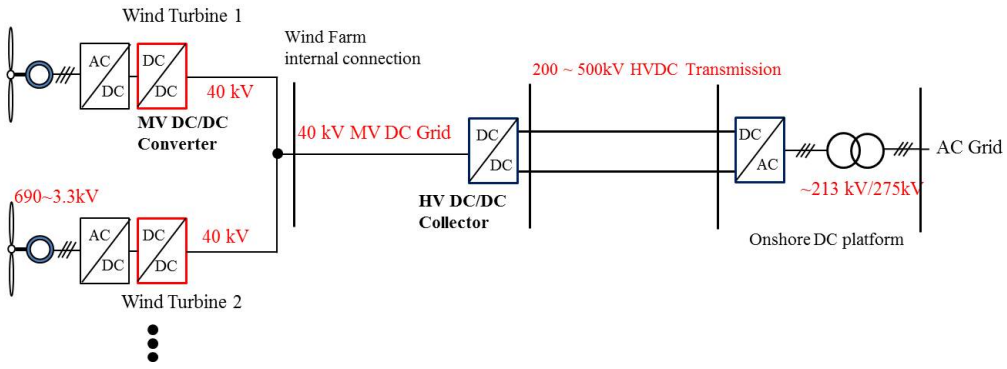


Fig. 1: Configurations of DC Grid for offshore wind farm

Two Possible configurations as shown in Fig. 1 can be proposed for the DC grid connection. In these configurations, a PWM rectifier converts the output voltage of wind turbine into LVDC level and a

MV DC-DC converter is located in the wind turbine platform to boost the LV level to MVDC line. In the MVDC line, additional wind turbines can be equipped for power collection. , the collection MV level is boosted up to HVDC transmission level by a high voltage (HV) DC-DC converting platform. High-power DC-DC converters are one of main technologies to interconnect with DC grids [4-9]. The 3DAB Converter, which is suitable for high-power application, has been studied in [6-9]. 3DAB converter topology is depicted in Fig. 2. The power can be transferred by phase shift angle $\varphi$ between the primary and secondary terminals voltage of the transformer. This paper aims at design and analysis of a high-power 3DAB converter for MVDC grids. The derivation of a generalized steady-state model of the 3DAB converter by using First Harmonic Approximation (FHA) method is described briefly to help understand the large-signal operation. An optimal phase shift control strategy is also presented to make the improvement of the efficiency. Two cases of the 4MW converter topology are compared in terms of losses of all semiconductor devices and magnetic component.

## FHA modelling of 3DAB DC-DC Converter

Switched transformer currents can be simplified by considering only the fundamental components based on First Harmonic Approximation (FHA) method [7]. In a 3DAB, the switched current at the transformer winding can be introduced by generated six-step voltage waveforms.

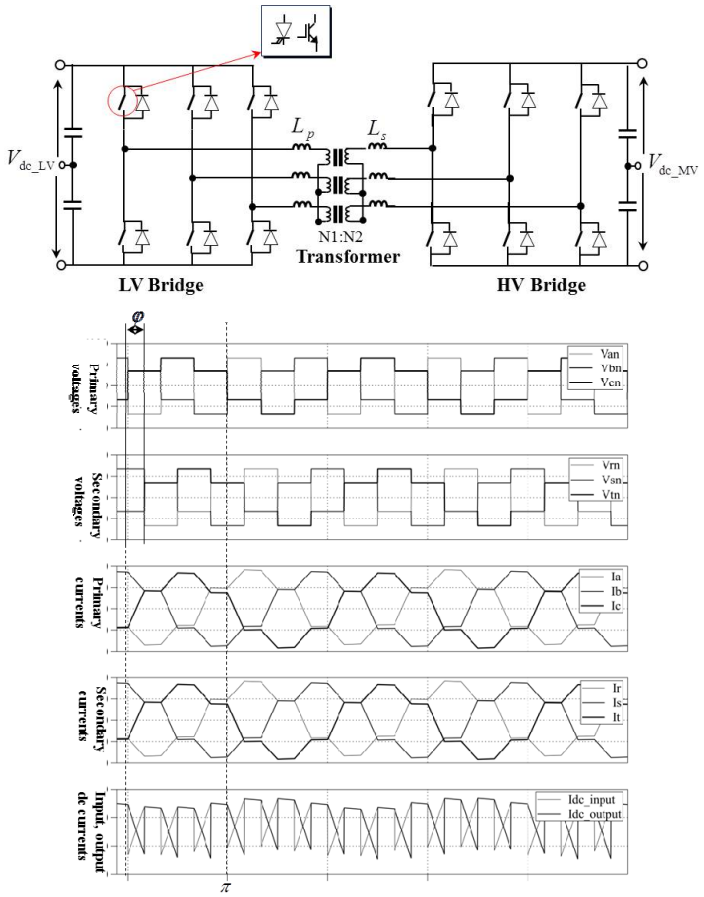


Fig. 2: A 3DAB DC-DC Converter topology

From each time interval, using the FHA method for the 3DAB which has been carried out in [7], the switched currents of primary $i(0)$ and secondary $i(\varphi)$ windings for steady-state analysis can be calculated by as

$$i(0)=\frac{V_{in}}{3\omega_{sw}L_{\sigma}}\left[\frac{2}{3}\pi d-d\varphi-\frac{2}{3}\pi\right] \qquad \text{for}\left(0\le\varphi\le\pi/3\right)$$
$$i(0)=\frac{V_{in}}{3\omega_{sw}L_{\sigma}}\left[\pi d-2d\varphi-\frac{2}{3}\pi\right] \qquad \text{for}\left(\pi/3\le\varphi\le 2\pi/3\right) \tag{1}$$

$$i(\varphi)=\frac{V_{in}}{3\omega_{sw}L_{\sigma}}\left[\frac{2}{3}\pi d+\varphi-\frac{2}{3}\pi\right] \qquad \text{for}\left(0\le\varphi\le\pi/3\right)$$
$$i(\varphi)=\frac{V_{in}}{3\omega_{sw}L_{\sigma}}\left[\frac{2}{3}\pi d+2\varphi-\pi\right] \qquad \text{for}\left(\pi/3\le\varphi\le 2\pi/3\right) \tag{2}$$

RMS values of phase current at primary side of the transformer can be computed from the following

$$I_{prms}=\frac{V_{in}}{6\pi\cdot f_{sw}\cdot L_{\sigma}}\cdot\varphi\cdot\sqrt{\frac{2\pi-\varphi}{\pi}} \quad \text{for}\left(0\le\varphi\le\pi/3\right) \tag{3}$$

$$I_{prms}=\frac{V_{in}}{12\pi\cdot f_{sw}\cdot L_{\sigma}}\cdot\varphi\cdot\sqrt{\frac{8\pi-6\varphi}{\pi}} \quad \text{for}\left(\pi/3\le\varphi\le 2\pi/3\right) \tag{4}$$

The average output power is given by

$$P_o=\frac{V_{in}^2}{\omega_{sw}L_{\sigma}}\cdot d\cdot\varphi\left[\frac{2}{3}-\frac{\varphi}{2\pi}\right] \quad \text{for}\left(0\le\varphi\le\pi/3\right) \tag{5}$$

$$P_o=\frac{V_{in}^{\ 2}}{\omega_{sw}L_{\sigma}}d\left[\varphi-\frac{\varphi^2}{\pi}-\frac{\pi}{18}\right] \quad \text{for}\left(\pi/3\le\varphi\le 2\pi/3\right) \tag{6}$$

Finally, substituting the RMS currents and $V_{pn}=\frac{\sqrt{2}}{3}V_{in}$ into equation $S_T=3\cdot V_{pn}\cdot I_{prms}$, the required apparent power of the transformer can be calculated for a transformer design.

$$S_T=3\cdot V_{pn}\cdot I_{prms}=\frac{\sqrt{2}\cdot V_{in}^2}{6\pi\cdot f_{sw}\cdot L_{\sigma}}\cdot\varphi\cdot\sqrt{\frac{2\pi-\varphi}{\pi}} \quad \text{for}\left(0\le\varphi\le\pi/3\right) \tag{7}$$

$$S_T=\frac{\sqrt{2}\cdot V_{in}^2}{12\pi\cdot f_{sw}\cdot L_{\sigma}}\cdot\varphi\cdot\sqrt{\frac{8\pi-6\varphi}{\pi}} \quad \text{for}\left(\pi/3\le\varphi\le 2\pi/3\right) \tag{8}$$

## Optimal Phase Shift Angle

Stray inductance ($L_{\sigma}$) influences the performance of the 3DAB converter. The inductance value is defined by geometric parameter of transformer design. For example, a lower inductance gives wide operation range of soft switching. However it produces higher currents. Consequently, it can lead to high losses and ripple current in the dc input and output current. Furthermore, $L_{\sigma}$ also has impact on the calculation of required control phase shift angle. In this case, using equation (5), the equation (9) in terms of optimized $L_{\sigma}$ and converter operating parameters has been calculated for a maximum control phase shift angle requirement of $\varphi\le\pi/3$ in order to reduce maximum turn-off currents under rated operating conditions.

$$\varphi=\frac{2\pi}{3}-\sqrt{\left(\frac{2\pi}{3}\right)^2-2\pi\cdot\frac{P_o\cdot\omega_{sw}\cdot L_{\sigma}}{V_{in}\cdot V'_{out}}} \tag{9}$$

## Transformer Design and Optimization

One of key parts for the 3DAB Converter is a high-power galvanic transformer. The detailed description of a design and optimization method of the transformer operating on medium-frequency range can be found in [10]. Fig. 3 shows a 3DAB converter transformer design optimization algorithm evaluating designs to find an optimal design based on a defined objective function. To start the transformer design process, a 3DAB converter model is simulated with defined basic parameters. Accepted geometric designs with calculated stray inductance are validated using 2D transient Finite Element Analysis (FEA) in the first step. Once the designs are satisfied with all the conditions, 3DAB converter simulation using PLECS [12] is carried out using the validated stray inductance and calculated control phase shift angle in order to generate actual distorted excitation waveforms. Using this actual waveform, a 2D FEA is performed to demonstrate the losses of the transformer for the actual 3DAB converter distorted waveforms. Also, a PLECS simulation is run to verify the losses of the 3DAB converter model. Finally, if the validated efficiency is greater than the target value, the design is saved or else discarded.

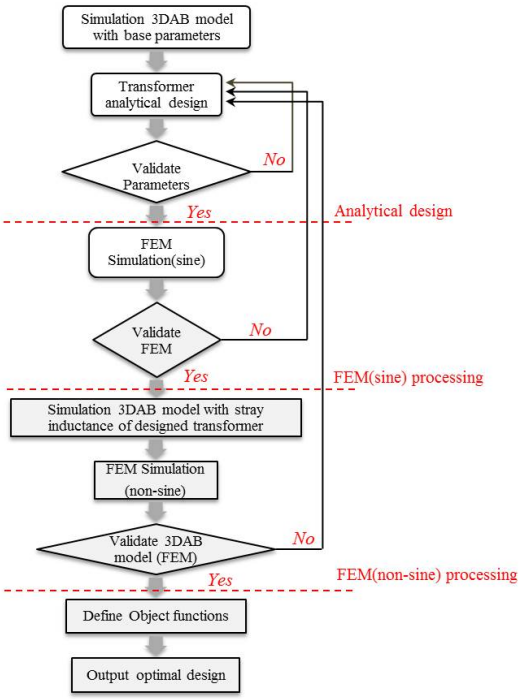


Fig. 3: Optimization Flowchart (From [10])

The conventional total copper losses is calculated as

$$P_{cu\_tot} = P_{cu\_p} + P_{cu\_s} = 3 \cdot \left( R_p \cdot I_{prms}^2 + R_s \cdot I_{srms}^2 \right) \tag{10}$$

where, $R_p$ is primary winding phase resistance, $R_s$ is secondary winding phase, $I_{prms}$ is primary winding rms current and $I_{srms}$ is secondary winding rms current. Core losses can be expressed using a Steinmetz equation. The core loss [W/kg] consists of hysteresis and eddy current losses given as

$$P_{s0} = \underbrace{k_h \cdot f_{sw}{}^{\alpha} \cdot B_m{}^{\beta}}_{\text{hysteresis}} + \underbrace{k_e \cdot \left( f_{sw} \cdot B_m \right)^2}_{\text{eddy current}} \tag{11}$$

Finally, the total core loss can be determined using the weight of the core as follow

$$P_s = P_{s0} \cdot weight_{core} = P_{s0} \cdot \rho_s \cdot vol_{core} \tag{12}$$

Where, $\rho_s$ is mass density of core material given from manufacturer and $vol_{core}$ is core volume in $m^3$. 2D FEA simulated time average total losses of core and windings for both 1.1kVDC and 5.2kVDC rated input voltages are shown in Fig. 4 respectively.

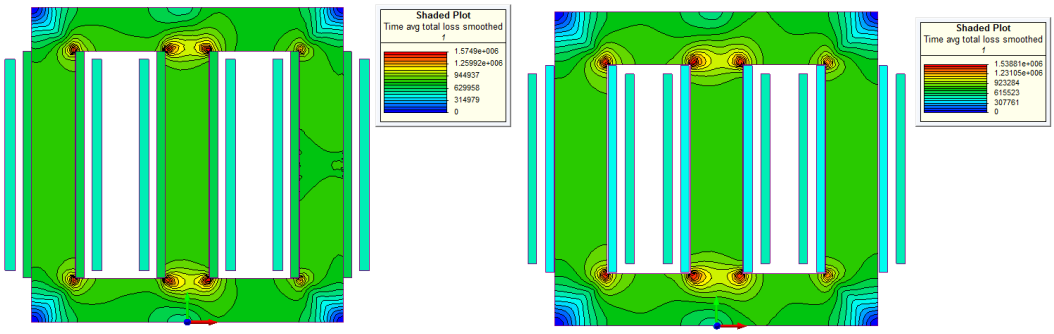


(a) (b)

Fig. 4: Average total losses of the transformer using 2D FEA simulation: (a) for 1.1kVDC rated voltage 3DAB converter (b) for 5.2kVDC rated voltage converter under non-sinusoidal excitation

## Considerations of high power semi-conductors

Since medium-voltage system applications are considered, insulated-gate bipolar transistor (IGBT) and integrated gate commutated thyristor (IGCT) are the suitable devices for the converter. In general, thyristor-based devices can be suggested for soft-switching due to lower conduction losses than IGBTs.

(a) (b) (c)

Fig. 5: high power semi-conductors: (a) Asymmetric IGCT, (b) StakPck IGBT module, and (c) HiPak IGBT module (Source: ABB [11])

For loss calculations, the characteristics of the IGCT are applied with fast recovery diode. Instantaneous conduction loss of IGCT can be calculated by:

$$P_{con\_igct}(t) = v_T \cdot i_T(t) = v_{T0} \cdot i_T(t) + r_T \cdot i_T^2(t) \tag{13}$$

Instantaneous conduction loss of Diode can be calculated by:

$$P_{con\_d}(t) = v_F \cdot i_F(t) = v_{F0} \cdot i_F(t) + r_T \cdot i_F^2(t) \tag{14}$$

Where, $v_T$ and $v_F$ are the calculated on-state voltages of IGCT and diode respectively. Threshold voltages $v_{T0} = 1.66V$ for IGCT, $v_{T0} = 1.70V$ for diode and slope resistances $r_T = 0.620m\Omega$ for IGCT, $r_T = 0.80m\Omega$ for diode are given from the datasheets. Fig. 6 shows instantaneous conduction loss curve of semi-conductor devices on primary side bridge of a 3DAB converter to transfer 4MVA of power for an input (LV) voltage of 1.1 kV and a nominal output (HV) voltage of 40 kV. At this operating condition, *d* is assumed to be 1 and $\phi = \pi/3$ is applied.

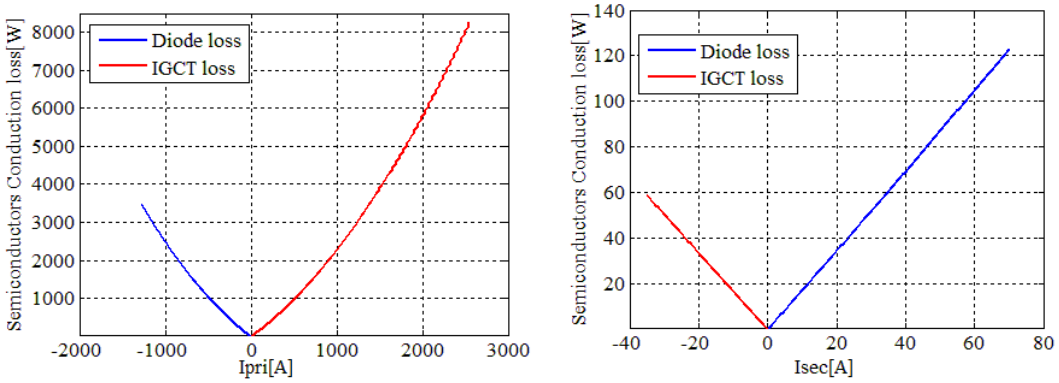


(a) (b)

Fig. 6: Instantaneous conduction loss versus (a): primary side switched current and (b): secondary side switched current

The conduction loss is determined by applying the operating condition to the equations derived from the steady-state model of the inductance current. Average conduction losses can be calculated by:

$$P_{avg\_con\_igct}(t) = \frac{1}{T_{sw}} \int_0^{T_{sw}} (v_{T0} \cdot i_c(t) + r_T \cdot i_c^2(t)) d = v_{T0} \cdot I_{avg\_igct} + r_T \cdot I_{rms\_igct}^2 \tag{15}$$

$$P_{avg\_con\_diode}(t) = \frac{1}{T_{sw}} \int_0^{T_{sw}} (v_F \cdot i_D(t) + r_T \cdot i_D^2(t)) dt = v_F \cdot I_{avg\_diode} + r_T \cdot I_{rms\_diode}^2 \tag{16}$$

During the switching process of the semi-conductor, a significant amount of the stored energy in the switch capacitance may be transferred from the switch to another hence, the switching losses amount to a significant part of the total losses. In steady-state operation, each switch of the 3DAB converter is turned-on and turned-off during one half-cycle respectively. If the 3DAB converter operates in zero voltage switching (ZVS) range, turn-on losses of the semi-conductors can be eliminated. In the ZVS operation, conduction and turn-off switching losses can be expected to contribute the main factor of semi-conductor losses. In the future step, an analysis of switching loss in each hard-switching and soft-switching range will be required in order to accurately determine the power dissipated in the semi-conductor. In this paper, a simple calculation is applied to estimate the loss during the ZVS operation. Turn-off loss is calculated from the turn-off energy loss curve given in the datasheet for the corresponding turn-off current and voltage. The total switching losses are calculated by summing the losses of the individual switching events

$$P_{sw\_off} = \frac{1}{t_{off}} \sum E_{OFF} \tag{17}$$

Similarly, the calculation of the turn-on loss corresponds to the turn-off loss

$$P_{sw\_on} = \frac{1}{t_{on}} \sum E_{ON} \tag{18}$$

Average switching losses of IGCTs and Diodes are calculated from

$$P_{sw\_LV} = n\left[ (E_{OFF\_igct} + E_{OFF\_diode}) \times f_{sw} \times \frac{V_{CE}}{V_{CC}} \right] \tag{19}$$

$$P_{sw\_HV} = n\left[ (E_{OFF\_igct} + E_{OFF\_diode}) \times f_{sw} \times \frac{V_{CE}}{V_{CC}} \right] \tag{20}$$

Where, $n$ is the number of devices, $f_{sw}$ is the switching frequency, $V_{CE}$ is the operating voltage, and $V_{CC}$ is the maximum voltage defined from the energy loss curves. Fig. 7 shows analysed turn-off losses in J of selected high-power IGCT and IGBT devices for the two scenarios. Turn-off losses $E_{OFF}$ are valid at the selected value of the 3DAB converter currents and at the limited devices' junction temperature ($T_j = 125°C$).As can be found from Fig. 7 (a), the asymmetric IGCT device with higher voltage rating is in tendency worse than the Hipak IGBT device. However, for an equal voltage level assessment as Fig. 7(b), the 4.5kV IGCT device allows to select more efficient devices with respect to the target rating power than the HiPak IGBT device. In case of 40kVDC application, depicted in Fig. 7(c), it indicates also that the 5.5kV IGCT device requires increased device physical layout resulting in higher switching losses than the 4.5kV StakPak IGBT device.

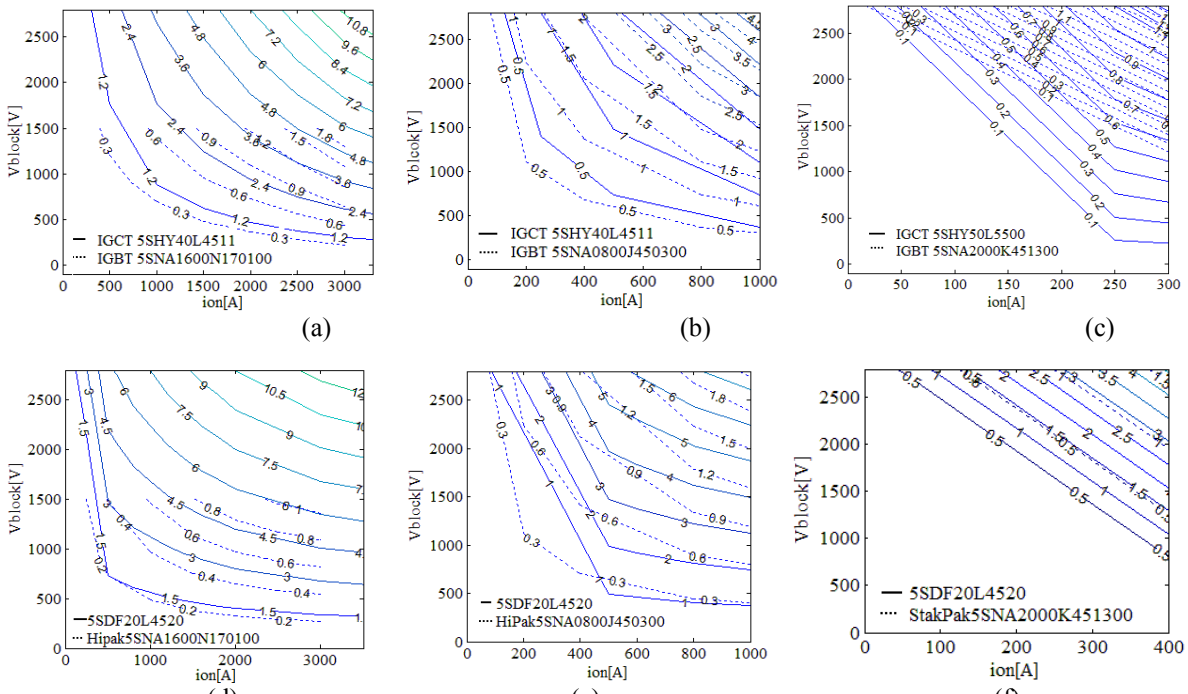


Fig. 7: Turn-off losses in J of high power semi-conductors: (a) active switches for 1.1kVDC level, (b) active switches for 5.2kVDC level, (c) active switches for 40kVDC level, (d) diodes for 1.1kVDC level, (e) diodes for 5.2kVDC level, (f) diode for 40kVDC level.

## Analysis of power losses of two scenarios for MVDC collector grid

In these scenarios, a MV DC-DC collector based on the 3DAB Converter operated with different nominal input voltages $V_{in}$ = 1.1kVDC and 5.2kVDC with a rated power of 4MW is interconnected with the MVDC grid. In two different scenarios, two MV DC-DC collectors applied by different semi-conductor devices are compared in terms of amount of semi-conductors, power losses and expense on transformer. For the given scenarios, the comparison of an appropriate high-voltage high-power IGBTs and IGCTs are carried out. To investigate these scenarios, high power density semi-conductors are considered as shown in Table I. Fig. 8 and 9 show connection of semi-conductors on the primary side (LV) converter. In scenario A, a total of 12 HiPak IGBT modules are applied in the primary bridge while 12 asymmetric IGCT modules are applied with 12 fast recovery diodes in the primary bridge. In scenario B, a parallel connection of semi-conductors is not compared due to the low current. However, a series connection of semi-conductors is required at high voltage. The secondary bridge

that operates on 40kVDC requires 108 StakPak IGBT modules to achieve the MV level in IGBTs based converter. On the other hand, the secondary bridge requires 96 asymmetric IGCT modules with fast recovery diodes in IGCTs based system due to high voltage capability of the IGCTs.

**Table I: Circuit parameters of the converters for the given scenarios**

| | | Scenario A | Scenario B |
|---|---|---|---|
| Input Voltage [kDC] | | 1.1 | 5.2 |
| Output Voltage [kDC] | | 40 | |
| Switching Frequency [kHz] | | 1 | |
| Stray Inductance [uH] | | 10.79 | 178.71 |
| Control Phase Shift Angle | | 21° | 15° |
| **IGBT based** | Primary bridge | ABB Hipak 5SNA 1600N170100[11] | ABB HiPak 5SNA 0800J450300[11] |
| | Secondary bridge | ABB StakPak 5SNA 2000K451300[11] | |
| **IGCT based** | Primary bridge | ABB asymmetric IGCT 5SHY40L4511[11] Diode 5SDF20L4520[11] | |
| | Secondary bridge | ABB asymmetric IGCT 5SHY50L5500[11] Diode 5SDF20L4520[11] | |

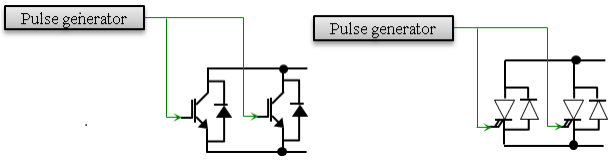


Fig. 8: Active switching device configurations of primary side converter at 1.1kVDC$_{input}$

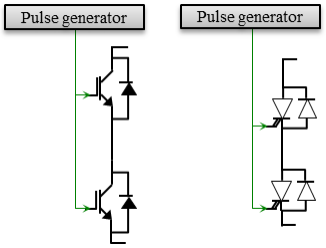


Fig. 9: Active switching device configurations of primary side converter at 5.2kVDC$_{input}$

The results take conduction losses and switching losses of the semi-conductors into account as well as core losses and winding losses of the transformers. To verify the analytical calculation of the semi-conductor losses, the scenarios have been built up in PLECS. The breakdown of losses in Fig. 10 show increasing semi-conductor losses (switching loss and conduction loss) with transferred power, whereas the percentage of the transformer losses are smaller. For the IGCTs based 3DAB converter, the diagrams show a slightly lower efficiency than the IGBTs based converter in the scenario A. However, the IGCTs based converter show a better performance if the converter is operated in scenario B. At full load, the efficiency of IGCTs based converter is about 98.2 % while the losses of the IGBTs based converter are higher at this point leading to a lower efficiency of about 97.4% due to high switching losses in scenario B. As with both scenarios, the MV DC-DC collector based on the two different semi-conductors can be operated with above 97 % efficiency. At load is 25%, core loss is considered as the main part of the power dissipation for the MV DC-DC collector. In the case of 40kVDC grids, the IGBTs based converter requires a slightly higher quantity of semi-conductors. Consequently, the efficiency of the IGBTs based converter becomes lower than the efficiency of the 3DAB converter

designed by IGCT device. In the 1.1kVDC primary side converter, however, it has been shown that the condition performance of the IGBTs is higher compared to the condition performance of the IGCTs, because the switching loss of the IGCTs becomes high resulting in a low efficiency. Legend information for loss distribution diagrams of simulation results is illustrated as below.

- Core : Transformer core loss,
- Cu_pri : Transformer primary winding loss
- Cu_sec : Transformer secondary winding loss
- S_IGBTp : IGBT switching losses on primary side
- C_IGBTp : IGBT conduction losses on primary side
- S_IGBTs : IGBT switching losses on secondary side
- C_IGBTs : IGBT conduction losses on secondary side
- S_IGCTp : IGCT switching losses on primary side
- C_IGCTp : IGCT conduction losses on primary side
- S_IGCTs : IGCT switching losses on secondary side
- C_IGCTs: IGCT conduction losses on secondary side
- C_Dp : Diode conduction losses on primary side
- C_Ds : Diode conduction losses on secondary side

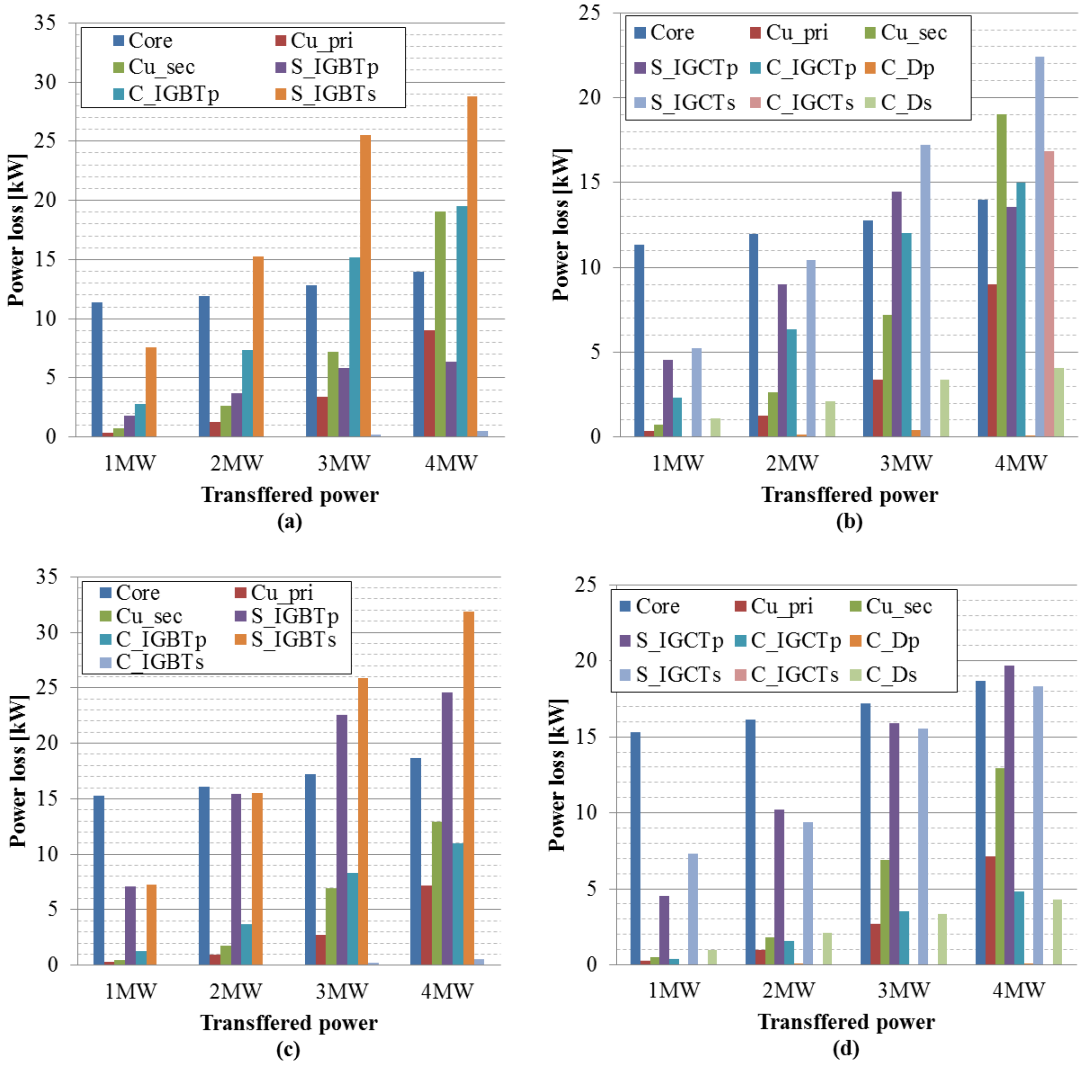


Fig.10: Loss distributions: (a) Scenario A with IGBTs based converter, (b) Scenario A with IGCTs based converter, (c) Scenario B with IGBTs based converter, and (d) Scenario B with IGCTs based converter

## Conclusion

In this paper, a FHA modelling and a design consideration of a 3DAB DC-DC converter for MVDC grids has been presented. Stray inductance can be calculated by the proposed design procedure of a transformer and optimized to calculate an optimal phase sift angle to reduce power losses of semi-conductors. IGCTs and IGBTs based converters have been investigated for different scenarios employing 40kVDC grids for offshore wind farms in terms of losses of the converters under steady-state condition. Finally, the validity of the results shows that IGCTs are optimal switch devices for higher voltage application.

## Nomenclature

| | | |
|---|---|---|
| $\varphi$ | Phase shift angle | [rad] |
| $\omega_{sw}$ | Switching frequency | [rad/s] |
| $d$ | DC conversion ratio | |
| $k_h$ | Coefficient for hysteresis losses | |
| $k_e$ | Coefficient for eddy current losses | |
| $B_m$ | Peak flux density | [T] |

## References


[1] D. Jovcic and N. Strachan.: Offshore wind farm with centralised power conversion and DC interconnection, in IET Generation, Transmission & Distribution, Vol. 3, no. 6, pp. 586-595, June 2009.

[2] S. Rodrigues, R. Teixeira Pinto, P. Bauer, E. Wiggelinkhuizen and J. Pierik.: Optimal power flow of VSC-based multi-terminal DC networks using genetic algorithm optimization, 2012 IEEE Energy Conversion Congress and Exposition (ECCE), Raleigh, NC, 2012, pp. 1453-1460.

[3] D. Jovcic, D. van Hertem, K. Linden, J. P. Taisne and W. Grieshaber.: Feasibility of DC transmission networks, Innovative Smart Grid Technologies (ISGT Europe), 2011 2nd IEEE PES International Conference and Exhibition on, Manchester, 2011, pp. 1-8.

[4] A. J. Watson, P. W. Wheeler and J. C. Clare.: Field programmable gate array based control of Dual Active Bridge DC/DC Converter for the UNIFLEX-PM project, Power Electronics and Applications (EPE 2011), Proceedings of the 2011-14th European Conference on, Birmingham, 2011, pp. 1-9.

[5] M. N. Kheraluwala, R. W. Gascoigne, D. M. Divan and E. D. Baumann.: Performance characterization of a high-power dual active bridge DC-to-DC converter, in IEEE Transactions on Industry Applications, vol. 28, no. 6, pp. 1294-1301, Nov/Dec 1992.

[6] R. L. Steigerwald, R. W. De Doncker and H. Kheraluwala.: "A comparison of high-power DC-DC soft-switched converter topologies, in IEEE Transactions on Industry Applications, vol. 32, no. 5, pp. 1139-1145, Sep/Oct 1996.

[7] R. W. A. A. De Doncker, D. M. Divan and M. H. Kheraluwala.: A three-phase soft-switched high-power-density DC/DC converter for high-power applications, in IEEE Transactions on Industry Applications, vol. 27, no. 1, pp. 63-73, Jan/Feb 1991.

[8] S. P. Engel, M. Stieneker, N. Soltau, S. Rabiee, H. Stagge and R. W. De Doncker, Comparison of the Modular Multilevel DC Converter and the Dual-Active Bridge Converter for Power Conversion in HVDC and MVDC Grids, in IEEE Transactions on Power Electronics, vol. 30, no. 1, pp. 124-137, Jan. 2015.

[9] N. Soltau, H. Stagge, R. W. De Doncker and O. Apeldoorn.: Development and demonstration of a medium-voltage high-power DC-DC converter for DC distribution systems, 2014 IEEE 5th International Symposium on Power Electronics for Distributed Generation Systems (PEDG), Galway, 2014, pp. 1-8.

[10] Y. S. Lee, G. Vakil, R. Feldman, A. Goodman, and P. Wheeler.: Design Optimization of a High-Power Transformer for Three-Phase Dual Active Bridge DC-DC Converter for MVDC Grids, Power Electronics, Machines and Drives (PEMD 2016), 8th IET International Conference on, Glasgow, 2016.

[11] [Online]. Available: http://new.abb.com/semiconductors

[12] [Online]. Available: http://www.plexim.com/plecs